nature chemistry

ARTICLES

PUBLISHED ONLINE: 20 APRIL 2015 | DOI: 10.1038/NCHEM.2236

Functionalization of cobalt porphyrin–phospholipid bilayers with his-tagged ligands and antigens

Shuai Shao[1,2], Jumin Geng[1], Hyun Ah Yi[3], Shobhit Gogia[2], Sriram Neelamegham[2], Amy Jacobs[3] and Jonathan F. Lovell[1,2]*

Methods to attach polypeptides to lipid bilayers are often indirect and ineffective, and can represent a substantial bottleneck in the formation of functionalized lipid-based materials. Although the polyhistidine tag (his-tag) has been transformative in its simplicity and efficacy in binding to immobilized metals, the successful application of this approach has been challenging in physiological settings. Here we show that lipid bilayers containing porphyrin–phospholipid conjugates that are chelated with cobalt, but not with other metals, can effectively capture his-tagged proteins and peptides. The binding follows a Co(II) to Co(III) transition and occurs within the sheltered hydrophobic bilayer, resulting in an essentially irreversible attachment in serum or in a million fold excess of competing imidazole. Using this approach we anchored homing peptides into the bilayer of preformed and cargo-loaded liposomes to enable tumour targeting without disrupting the bilayer integrity. As a further demonstration, a synthetic protein fragment derived from the human immunodeficiency virus was bound to immunogenic liposomes for potent antibody generation for an otherwise non-antigenic peptide.

The development of targeted nanoparticles that nimbly guide payloads to diseased tissues[1] and the rational design of peptide antigens that induce the immune system to combat diseases[2] have been the focus of considerable research efforts. One bottleneck in advancing these techniques stems from difficulties in easily and reliably attaching peptides and proteins to larger scaffolds; targeted nanoparticles require effective ligands and the unconjugated peptides themselves are weakly immunogenic. Bioconjugate chemistry has provided a range of strategies[3], but most nanoparticulate conjugations suffer from limitations that relate to one or more of the following: (1) low conjugation yields and the necessitated purification steps; (2) incompatibility with biological buffers, which makes labelling of intact nanoparticles impossible; (3) variable labelling sites and conjugated polypeptide conformations, which create an inhomogeneous particle population with varying degrees of function; (4) the necessity for complex and exogenous chemical approaches[4].

Standard approaches for ligand attachment to aqueous nanoparticles make use of maleimides, succinimidyl esters and carboiimide-activated carboxylic acids[5]. These can covalently react with the amine and thiol groups of polypeptides. The use of maleimide lipids has been explored extensively for antibody-conjugated immunoliposomes[6]. Conjugation yields may reach as high as 90% from an overnight reaction, but subsequent quenching of the free maleimide groups and additional purification is required[7]. Proteins may require a preparative step of thiolation and purification prior to conjugation[8]. Antibody orientation is a major factor that influences the conjugated antibody target-binding efficacy, but these approaches result in numerous antibody labelling sites and indiscriminate orientations[9]. Biorthogonal synthetic strategies, such as the click reaction, have recently been applied to preformed liposomes; however, these require the use of exogenous catalysts and unconventional amino acids[10].

Another approach suitable for smaller peptides that are less prone to permanent denaturation in organic solvents is to conjugate the peptides to a lipid anchor. The resulting lipopeptides can then be incorporated along with the other lipids during the liposome-formation process. This approach has been used to generate synthetic vaccines that induce antibody production against otherwise non-immunogenic peptides[11]. However, their amphipathic character means that the lipopeptides are difficult to purify. It has also been shown that lipopeptides do not fully incorporate into liposomes during the formation process, which results in aggregation[12]. These problems necessitate evolving strategies to work with liposomal lipopeptides, such as adding multiple lipidation sites[13].

One alternative strategy of interest that could avoid these limitations is to adopt the non-covalent method used in immobilized metal ion affinity chromatography (IMAC)[14]. Polypeptides containing a polyhistidine-tag (his-tag) that comprises a stretch of approximately 6–10 consecutive histidine residues can be purified from a crude lysate using immobilized microparticles decorated with Ni, Zn or Co chelators, such as nitrilotriacetic acid (NTA). This approach has changed the face of biotechnology and is common practice for the purification of recombinant proteins[15,16]. Ni-NTA conjugated phospholipids, which were described over 20 years ago and are commercially available, have also been used to bind his-tagged proteins, but largely in the context of structural biology studies[17–19]. Unfortunately, the chelation of his-tagged proteins with various Ni-NTA lipids in nanoparticulate form is not stable in biological media such as serum[20,21]. Based on the suitability of lipids for use *in vivo* in the form of liposomes or as coatings for other nanoparticles[22], stable lipid-based polyhistidine binding could be enabling for applications in biological settings.

Porphyrin–phospholipid (PoP) conjugates have recently been developed that can self-assemble into biodegradable nanovesicles for multimodal imaging and phototherapy[23–26]. With four cyclic nitrogens, PoP conjugates also represent potent chelators for exactly the same transition metals as frequently used in IMAC. In this work, we demonstrate that a metallo-PoP bilayer specifically formed from cobalt porphyrin–phospholipid (Co-PoP) can stably

[1]Department of Biomedical Engineering, University at Buffalo, State University of New York, Buffalo, New York 14260, USA. [2]Department of Chemical and Biological Engineering, University at Buffalo, State University of New York. Buffalo, New York 14260, USA. [3]Department of Microbiology and Immunology, University at Buffalo, State University of New York, Buffalo, New York 14260, USA. *e-mail: jflovell@buffalo.edu

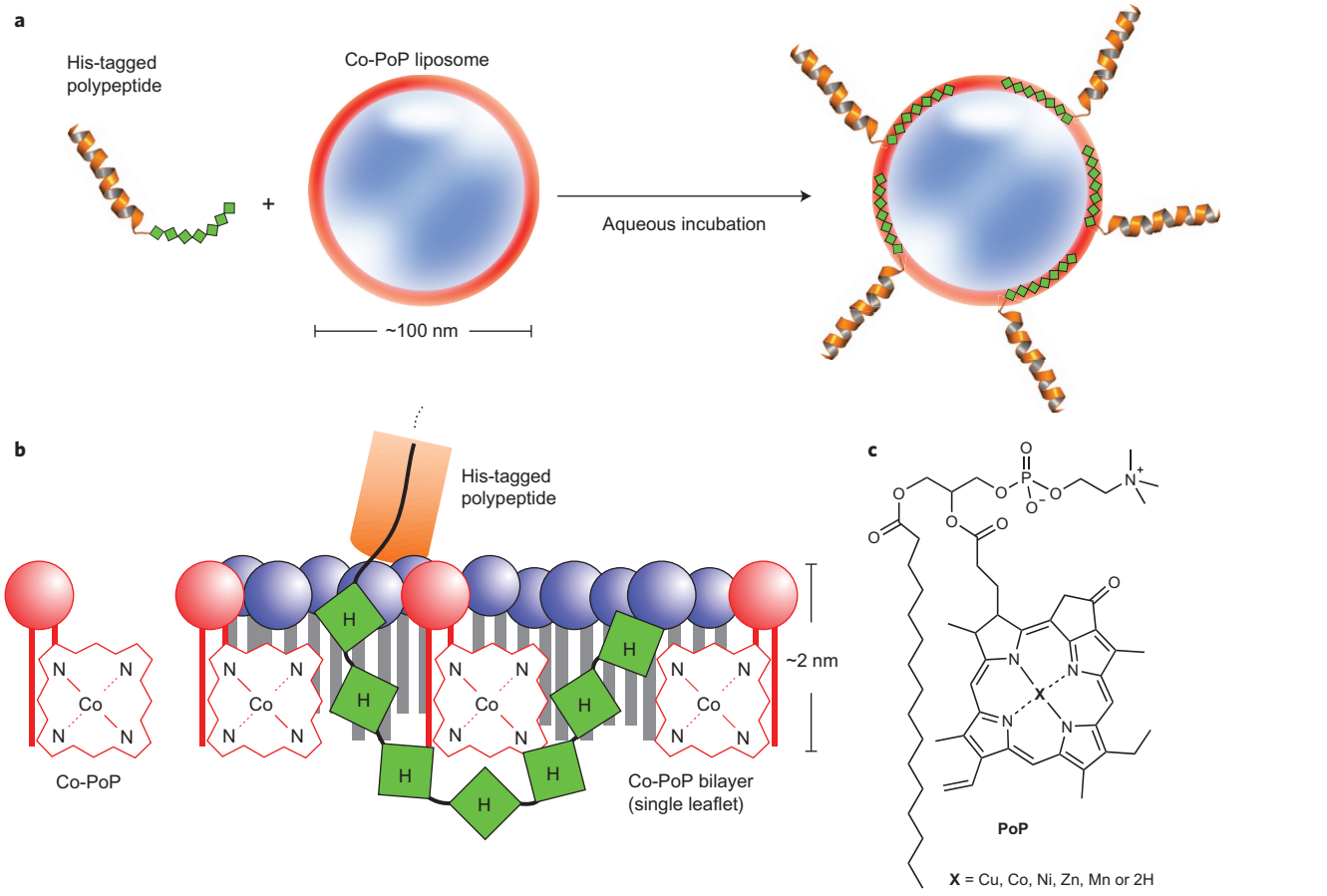

Figure 1 | His-tagged polypeptides bind and functionalize Co-PoP bilayers. a, Schematic that shows a peptide with a his-tag (green) binding to preformed Co-PoP liposomes in an aqueous solution. A simple aqueous incubation results in the insertion of the his-tag into the bilayer and stable binding. **b**, Insertion of a his-tagged polypeptide into a bilayer containing Co-PoP (red) along with a majority of conventional phospholipids (blue). Only a single leaflet of the bilayer is shown. The imidazole groups of the histidine residues coordinate with cobalt within the hydrophobic bilayer phase. **c**, Chemical structure of the metallo-PoPs used in this study.

bind his-tagged polypeptides with simple aqueous incubation (Fig. 1a). This represents a new binding model, with the polyhistidine buried in the membrane phase as the porphyrins themselves form the hydrophobic portion of the bilayer and are not accessible to the external aqueous environment (Fig. 1b). This leads to a more stable binding, allows for significantly simpler non-covalent post-labelling methods after the nanoparticle formation and eliminates ambiguity regarding ligand orientation.

Results and discussion

His-tagged protein binding to Co-PoP liposomes. A series of *sn*-1-palmitoyl *sn*-2-pyropheophorbide phosphtatidylcholine chelates was generated with the transition metals Co, Cu, Zn, Ni and Mn (Fig. 1c). PoP bilayers were then formed with 10 mol% metallo-PoP along with 85 mol% dioleoylphosphatidylcholine (DOPC) and 5 mol% polyethylene glycol-conjugated distearoylphosphatidylethanolamine (PEG-lipid) via extrusion into 100 nm liposomes. His-tagged protein binding to the PoP bilayers was assessed with a fluorescent protein reporter. As shown in Fig. 2a, the system comprised a fusion protein made up of two linked fluorescent proteins, Cerulean (blue emission) and Venus (green emission). Owing to their linked proximity and spectral overlap, Cerulean serves as a Förster resonance energy transfer (FRET) donor for Venus, so that the Cerulean excitation results in FRET emission from Venus. Cerulean was tagged at its C terminus with a heptahistidine tag. However, if bound to a PoP bilayer, energy transfer from Cerulean is diverted to the bilayer itself, which is absorbing in the Cerulean emission range and thus competes with the FRET to Venus. Also, as Venus is not directly attached to the photonic bilayer, it is not completely quenched on direct excitation, which enables tracking of the bound fusion protein.

A three-colour electrophoretic mobility shift assay (EMSA) was developed to assess reporter fusion protein binding to various PoP liposomes. Protein (2.5 μg) was incubated with 50 μg of various PoP liposomes for 24 hours and then subjected to agarose gel electrophoresis. As shown in the top image in Fig. 2b, when the PoP liposomes were imaged, only the free base (2H) liposomes were readily visualized, along with, to a lesser degree, the Zn-PoP liposomes. This demonstrates that the metals have a quenching effect on the PoP liposome and confirms they were stably chelated in the bilayer. As expected, the liposomes exhibited minimal electrophoretic mobility because of their relatively large size. Next, the same gel was imaged using Cerulean excitation and Venus emission to probe for the inhibition of FRET, which would be indicative of the fusion protein binding to PoP liposomes. All the samples exhibited the same amount of FRET and migrated the same distance as the free protein, with the exception of the protein incubated with Co-PoP liposomes, for which the FRET disappeared completely (middle image). To verify the presence of the protein, Venus was directly excited and imaged. Only with the Co-PoP liposomes was the reported protein colocalized with the liposomes. Together, these images demonstrate that the protein bound quantitatively to the Co-PoP liposomes. Solution-based studies confirmed this

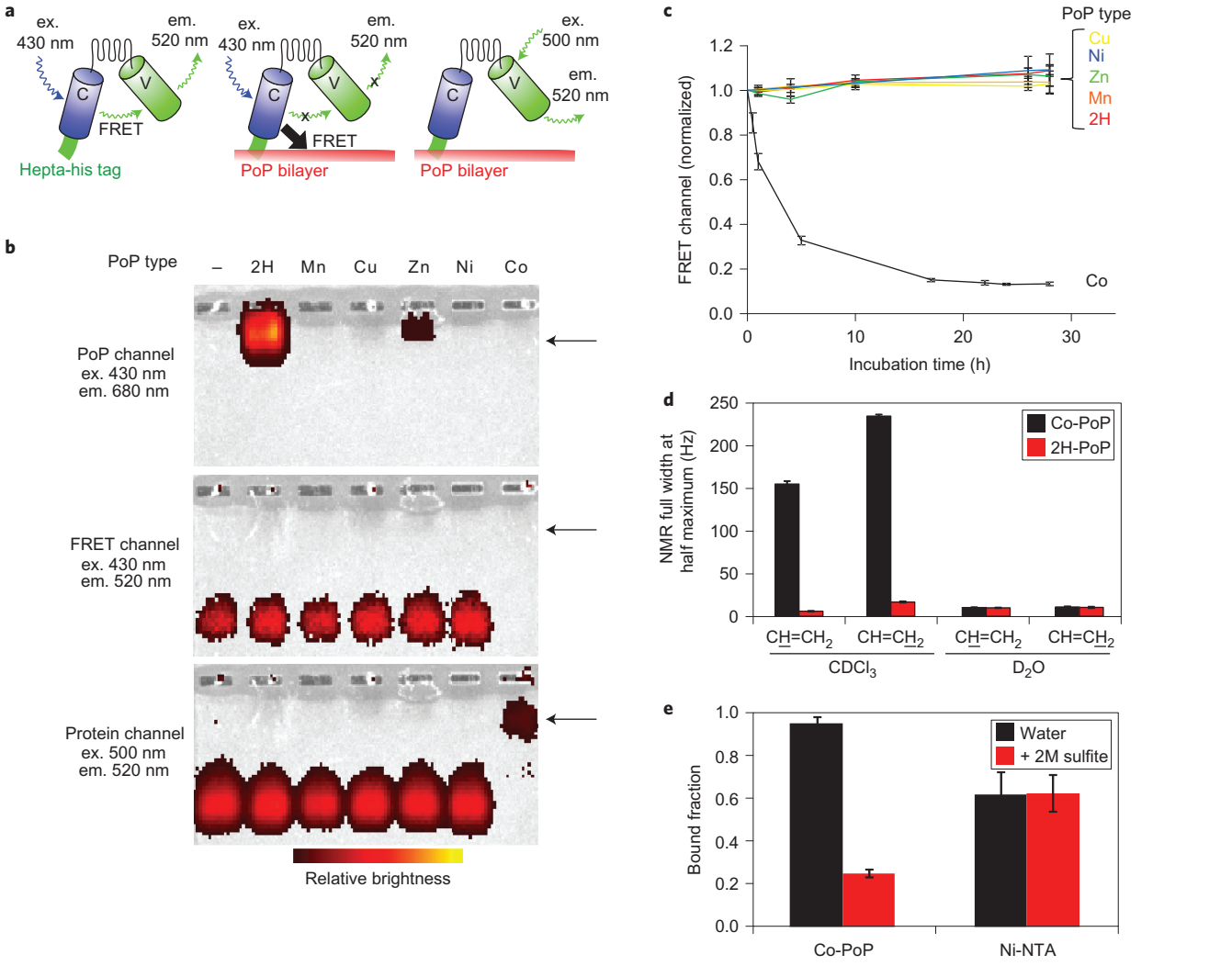

Figure 2 | His-tagged protein binding to Co(III)-PoP liposomes. a, A heptahistidine (hepta-his)-tagged fluorescence protein that comprises Cerulean (C) fused to Venus (V) reveals binding to the PoP bilayers. When C is excited, FRET occurs and V emits fluorescence (left), but this is inhibited when bound to the PoP bilayer because of FRET competing with the photonic bilayer (middle). The C fluorescence can be probed directly even when the protein is bound to the bilayer (right). **b**, Multispectral fluorescence images of a fusion protein electrophoretic mobility shift after incubation with the indicated metallo-PoP liposomes. Arrows indicate the position of the protein bound to Co-PoP liposomes. **c**, Binding kinetics of the fusion protein to the indicated metallo-PoP liposomes based on the loss of C to V FRET. **d**, NMR peak widths of the underlined proton of the vinyl group on Co-PoP demonstrate paramagnetic broadening of Co(II) in deuterated chloroform ($CDCl_3$) but non-paramagnetic peaks of Co(III) after Co-PoP liposome formation in deuterated water. **e**, Reversal of his-tagged peptide binding to Co-PoP liposomes after the addition of 2 M sodium sulfite. Liposomes were formed with 10 mol% Co-PoP or Ni-NTA phospholipid. All the graphs show the mean ± s.d. for $n = 3$. em, emission; ex, excitation.

finding (Fig. 2c). Of all the types of PoP liposomes examined, only the Co-PoP ones induced a dramatic decrease in the FRET efficiency between Cerulean and Venus, caused by the liposomal binding. The binding required approximately a day to complete fully, although the time to achieve a 50% binding ($t_{1/2}$) was just three hours. It was previously shown by molecular dynamics simulations of a freebase (2H) PoP (2H-PoP) bilayer that the centres of the porphyrins (where metal chelation would occur) are inaccessible to the aqueous phase that surrounds the bilayer[25]. Thus, this slow binding can be attributed to a his-tag that is partially obscured by the rest of the protein and has to make its way into the sheltered hydrophobic bilayer.

Polyhistidine coordination with Co-PoP. The mechanism that underlies his-tag binding to immobilized metals involves metal coordination with the nitrogenous imidazole groups of histidine residues. The absence of his-tag binding to liposomes formed with Ni(II), Cu(II), Zn(II) and Mn(II) PoP probably relates to an axial ligand-binding affinity or to the coordination number within the porphyrin. For instance, it has been proposed that Ni(II) and Cu(II) porphyrin chelates can coordinate completely with the four surrounding macrocyclic nitrogens without axial ligands[27]. For the Zn(II) and Mn(III) porphyrins, the ligand binding strength is probably insufficient to confer stable polyhistidine binding. The inorganic study of cobalt coordination was first pioneered by Werner over 100 years ago[28]. Co(III) complexes are of interest because they are often kinetically inert to ligand release and Co(III)-NTA has recently attracted interest for binding his-tag proteins with excellent stability[29]. Co(II) porphyrins, such as the originally synthesized Co-PoP, readily oxidize to Co(III) in aqueous solutions[30]. Confining Co(III)-mediated his-tag binding within a sheltered bilayer is expected to enhance further the binding stability in biological environments.

To determine the electronic state of the Co-PoP, its paramagnetism was assessed. As Co(II) is paramagnetic, but Co(III) porphyrins

are low spin and diamagnetic[30], NMR was used to probe for peak broadening induced by paramagnetic species. As shown in Fig. 2d, based on the hydrogens of each carbon of the vinyl group within the PoP, a wide peak broadening was observed only for the Co-PoP, and only in an organic solvent. When the Co-PoP was formed into aqueous liposomes, the peaks narrowed, which indicates oxidation to diamagnetic Co(III) within the bilayer. To verify this mechanism further, the reducing agent sodium sulfite was added to the Co-PoP liposomes after they were quantitatively bound to a fluorescently labelled his-tagged peptide. As shown in Fig. 2e, 2 M sulfite induced peptide release from the Co-PoP liposomes. Liposomes were also formed with a commercially available Ni-NTA lipid. The his-tagged peptide did not bind as avidly to the Ni-NTA liposomes. On the addition of sulfite to the system, no release of the peptide was observed, as expected with Ni(II), which cannot be reduced readily. Together, these data suggest that Co-PoP transitions from Co(II) to Co(III) on forming Co-PoP liposomes and the polyhistidine imidazole groups coordinate in the bilayer with chelated Co(III) in the PoP.

Stable his-tag binding to Co-PoP liposomes. The fluorescence reporter protein was then used to compare the binding of his-tagged proteins to liposomes that incorporated either Co-PoP or Ni-NTA lipid (Fig. 3a). The Ni-NTA liposomes included 10 mol% 2H-PoP to enable protein-binding determination based on FRET. By EMSA, the protein migrated unimpeded when incubated without liposomes or when incubated with 2H-PoP liposomes in both the FRET channel and the protein channel. When incubated with Ni-NTA liposomes, migration of the protein was only slightly inhibited, which indicates that the protein binding did not withstand the conditions of electrophoresis. That the FRET channel was unquenched confirmed a lack of binding to the Ni-NTA liposomes. In contrast, when incubated with the Co-PoP liposomes, the protein was bound stably, with the complete disappearance of the FRET channel and a decreased electrophoretic mobility that is consistent with the protein remaining bound to liposomes.

For biomedical applications, an intractable obstacle of using an Ni-NTA lipid is that it does not maintain stable his-tag binding in biological media such as serum[20,21]. To examine whether liposomes could maintain binding in the presence of serum, fetal bovine serum (FBS) was added at a 1:1 volume ratio to a solution of liposomes that had bound the his-tagged protein. As shown in Fig. 3b, Ni-NTA liposomes did not fully sequester all the protein, which is consistent with the weak binding exhibited in the EMSA result. After the serum addition, all the binding was abrogated over a 24 hour period. Under the same conditions Co-PoP liposomes stably sequestered the his-tagged reporter protein without substantial protein release.

As the histidine side chain comprises an imidazole group, an imidazole competition assay was used to compare the Ni-NTA and Co-PoP liposome binding stability with his-tagged polypeptides. As shown in Fig. 3c, Co-PoP liposomes maintained an over 75% binding to the reporter protein, even at concentrations that approached 1 M imidazole. This represents an approximate ten million fold imidazole excess over the 100 nM protein concentration used in the binding study. In contrast, the Ni-NTA liposomes released over 90% of the his-tag in the presence of just 30 mM imidazole. The drastically stronger binding of the Co-PoP liposome to the his-tag may be attributed to at least two factors: the superior stable chelation of Co(III) to imidazole groups and the protected hydrophobic environment of the Co-PoP bilayer, which limits access to competing external molecules.

Liposomes formed with the Ni-NTA lipid, the cobalt-chelated Co-NTA-lipid and the Co-PoP could bind a fluorescent peptide in solution (Supplementary Fig. 1a). However, the binding of

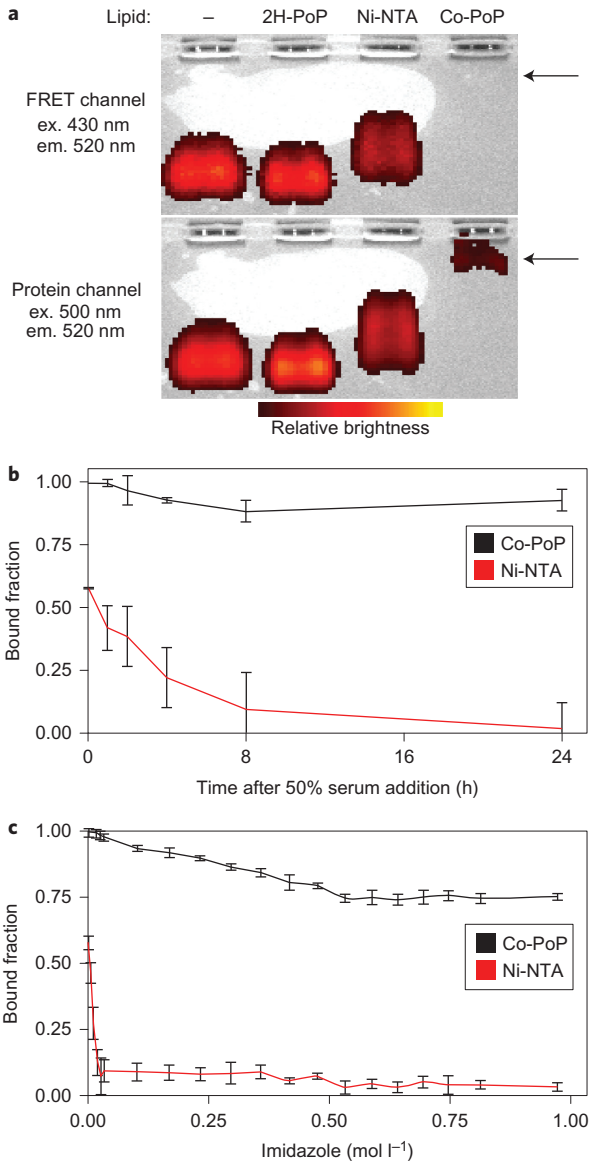

Figure 3 | Robust his-tagged protein binding to Co-PoP liposomes. **a**, Multispectral electrophoretic mobility shift images of the fluorescent reporter protein incubated with liposomes that contained the indicated lipid. The arrows point to the his-tagged protein bound to Co-PoP liposomes, which exhibit inhibited electrophoretic mobility because of the large size of the complex. 2H-PoP liposomes and Ni-NTA liposomes did not stably bind the protein. **b**, Binding stability of the reporter protein bound to the indicated liposomes after the addition of serum. **c**, Binding stability of the reporter protein bound to the indicated liposomes with excess free imidazole. All the graphs show the mean ± s.d. for $n = 3$.

Co-NTA and Ni-NTA was not maintained during gel-filtration chromatography (Supplementary Fig. 1b). Liposomes formed with Co-NTA and Ni-NTA, but not with Co-PoP, released the peptide when incubated in serum (Supplementary Fig. 1c). This demonstrates the significance of bilayer-confined polyhistidine binding. We next examined whether or not Co-PoP was required for a stable binding in serum, or whether a simple liposome-inserted cobalt porphyrin would be sufficient. After the initial binding, incubation with serum caused the polypeptide to become displaced from the liposomes (Supplementary Fig. 2). This result is consistent with demonstrations that membrane-inserted porphyrins, but not PoPs, rapidly exchange with serum

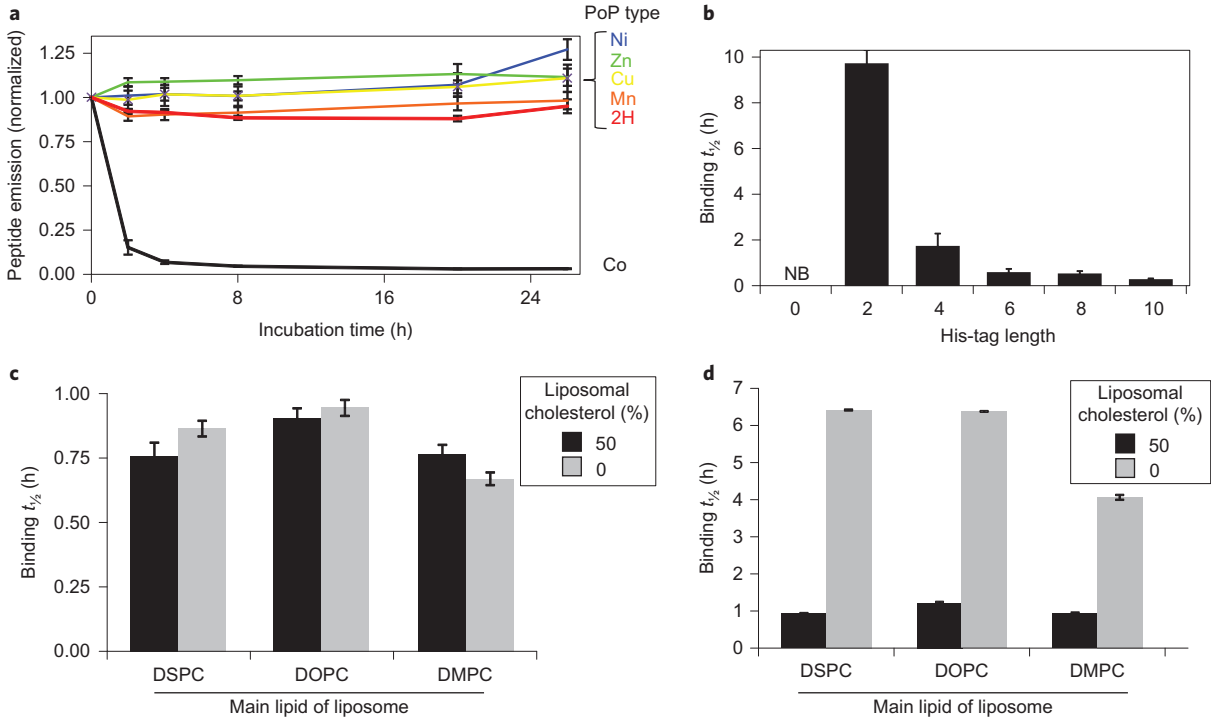

Figure 4 | Binding of a short his-tagged RGD peptide to Co-PoP liposomes. a, Binding of a short linear RGD-his peptide labelled with FAM to metallo-PoP liposomes. Only the Co-PoP liposomes bound the peptide. **b**, Effect of the his-tag length on binding $t_{1/2}$ to Co-PoP liposomes. No binding (NB) was observed for the peptide that lacked a his-tag. Increasing the his-tag length resulted in a faster binding. **c**,**d**, Effect of liposome composition on binding $t_{1/2}$ to Co-PoP liposomes of the indicated composition when incubated in PBS (**c**) or in 5 mg ml^{-1} BSA (**d**). In the presence of BSA, the binding was slower for liposomes that lacked cholesterol. All the graphs show the mean ± s.d. for $n = 3$.

components and exit the liposome[25]. Together these results point to the essential role Co-PoP plays to stably bind his-tagged polypeptides.

Peptide binding to Co-PoP liposomes. Peptide targeting has attracted interest for use as disease and tissue-specific 'zip codes'[31]. The short RGD tripeptide, which is found in fibronectin and vibronectin, is a promising targeting ligand for its effective binding to the integrin $\alpha_V\beta_3$ expressed on tumour endothelial cells[32,33]. Co-PoP liposomes were examined to verify whether they can be delivered to molecular receptors on target cells via a his-tagged ligand approach with the short linear amino-acid sequence GRGDSPKGAGAKG-HHHHHHH. Carboxyfluorescein (FAM) was labelled on the N terminus to enable the detection of binding to a PoP liposome via FRET. It has been shown that linear RGD peptides can be labelled with fluorophores without disrupting integrin binding[34]. As shown in Fig. 4a, when this peptide was incubated with various metallo-PoP liposomes, only the Co-PoP ones bound the peptide. Compared to protein binding, peptide binding was about five times faster. Presumably, the smaller size, faster molecular motion and decreased steric hindrance of the peptide enabled a more rapid interdigitation into the bilayer to interact with and irreversibly bind the Co-PoP. Based on previous estimates that each ~100 nm liposome contains approximately 80,000 lipids[7], this equates to 8,000 Co-PoPs and 750 peptides per liposome. As each peptide contained seven histidine residues, the ratio of Co-PoP to histidine in the bilayer was 1:0.66. This represents an excess of Co-PoP and, for conventional his-tag binding to Ni-NTA, of all the residues in the his-tag, only the *i*th and $i+2$ or $i+5$ histidine residues are believed to be involved in coordinating with the metal[14]. However, the porphyrin and polyhistidine density within the Co-PoP bilayer is probably higher and therefore the coordination mechanism may be different. Further work is required to determine the geometry and stoichiometry of his-tag binding in the Co-PoP bilayer phase.

The effect of his-tag length on peptide binding to the Co-PoP liposome was examined. A series of N-terminus FAM-labelled peptides was synthesized with varying lengths of his-tag attached to the C terminus. As demonstrated in Fig. 4b, when the his-tag was omitted from the peptide, no peptide binding was observed. With two histidine residues, the binding was slow, with a binding $t_{1/2}$ of nearly ten hours. As the his-tag length increased, the binding speed increased rapidly. With six residues, which corresponds to the common hexahistidine tag, the binding $t_{1/2}$ was less than one hour. By increasing the his-tag length to ten residues, the binding $t_{1/2}$ decreased to 20 minutes.

Next, the lipid composition was varied to determine the effect of membrane fluidity on his-tag binding. Liposomes were formed with 90 mol% of either distearoylphosphatidylcholine (DSPC), dimyristoylphosphatidylcholine (DMPC) or DOPC along with 10 mol% Co-PoP. Alternatively, 50 mol% cholesterol was also incorporated in the bilayer with a corresponding reduction in the amount of standard lipid used. DSPC forms rigid, gel-phase bilayers at room temperature, whereas DMPC and DOPC have lower transition temperatures and are in the liquid-crystal phase at room temperature. Cholesterol occupies space in the bilayer and can have a moderating effect on the membrane fluidity. Interestingly, no major differences were observed in the peptide-binding rate to membranes of different compositions, with or without cholesterol, with binding $t_{1/2}$ values of under one hour (Fig. 4c) and the times required for binding 90% of the peptide being between 10 and 12 hours (Supplementary Fig. 3). The peptide-binding process might be a multistep one so that, once the peptide begins insertion into the bilayer, cooperative effects of the polyhistidine are minimally impacted by lipid composition and fluidity. In the presence of 5 mg ml^{-1}

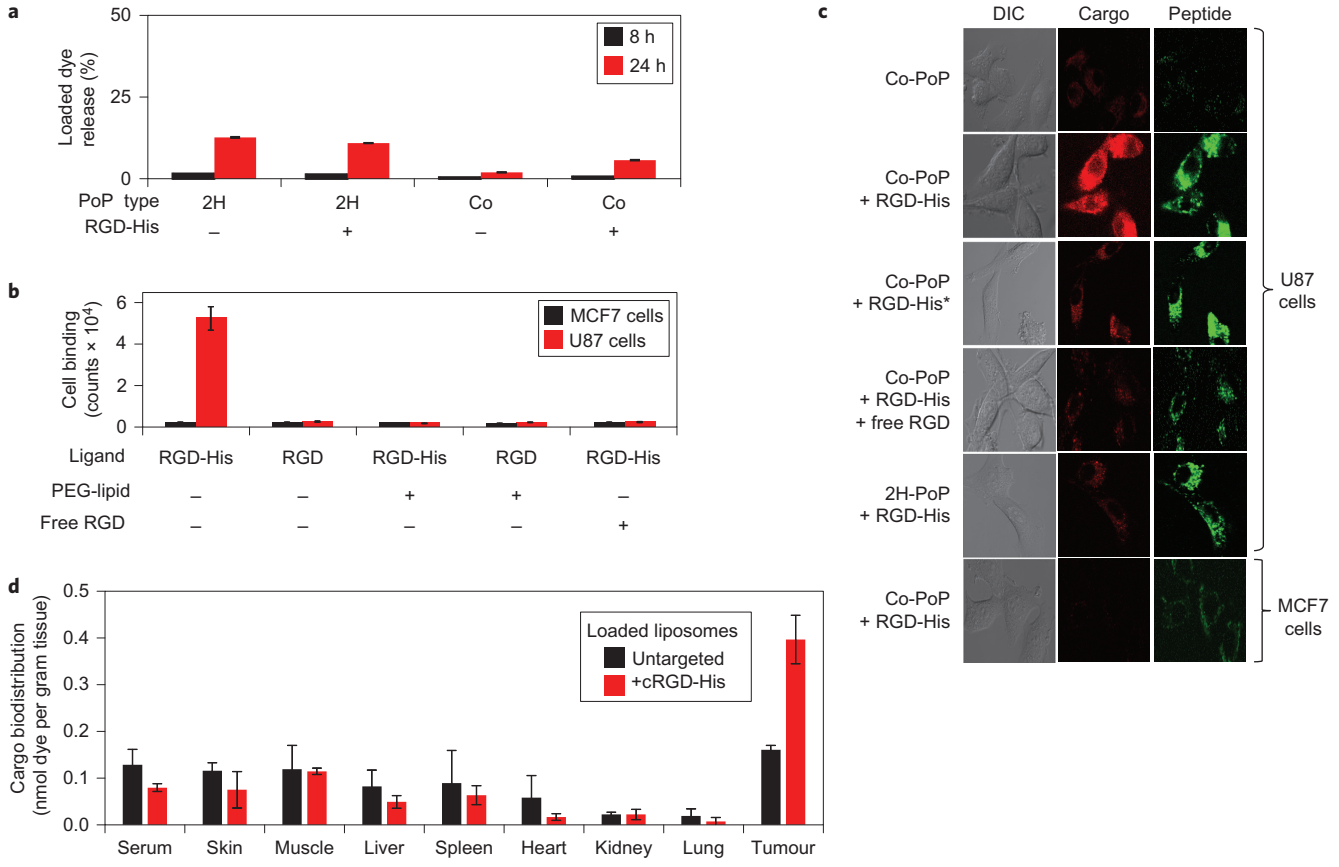

Figure 5 | RGD-his targeting of cargo-loaded liposomes. a, Release of entrapped sulforhodamine B in preformed PoP liposomes. Minimal membrane destabilization occurred in the process of his-tagged peptide functionalization. **b**, Targeted uptake of liposomes loaded with sulforhodamine B in U87 cells known to express $\alpha_V\beta_3$ or MCF7 control cells. Cells were incubated in the indicated conditions and uptake was assessed by examining sulforhodamine B fluorescence in cell lysates. **c**, Confocal micrographs that show the liposome uptake. The cells were incubated with the indicated liposome solutions for two hours, washed and imaged. All the images were acquired with the same settings. **d**, Biodistribution of sulforhodamine B entrapped in Co-PoP liposomes with or without the attachment of a his-tagged cyclic RGD-targeting peptide 45 minutes after intravenous injection into nude mice that bore subcutaneous U87 tumours. All the graphs show means ± s.d. for $n = 3$. *No preincubation.

bovine serum albumin (BSA), dramatic differences between the membranes with and without cholesterol were observed (Fig. 4d). The slower binding in cholesterol-free liposomes was probably because of a greater interaction of BSA with the membrane that interfered with peptide binding. Binding $t_{1/2}$ values were not reached with BSA at 50 mg ml^{-1} and serum completely inhibited binding (Supplementary Fig. 4).

Biotargeting of cargo-loaded liposomes. Given the binding efficacy of his-tagged peptides to Co-PoP liposomes, the bilayer integrity was assessed to determine whether peptide binding induces membrane destabilization. The aqueous core of liposomes was loaded with the fluorophore sulforhodamine B, a water-soluble dye, at self-quenching concentrations to probe for membrane permeabilization. As shown in Fig. 5a, dye-loaded liposomes did not release a substantial amount of dye over the eight hour period in which the peptide had fully bound to the liposomes. At 24 hours, the Co-PoP liposomes with the peptide bound released less than 10% of the dye. Thus, his-tag insertion and binding is sufficiently gentle and non-disruptive for the bilayer integrity and entrapped cargo to remain intact. The analogous palmitoylated lipopeptide resulted in permeabilization of the cargo-loaded liposomes on incubation (Supplementary Fig. 5), which further demonstrates the robustness of the his-tag approach.

Next, the liposomes were assessed for whether they could bind to their molecular targets with the established cell-line pair of U87 glioblastoma cells (RGD binding) and MCF7 breast-cancer cells (RGD non-binding)[35,36]. After sulforhodamine B entrapment, liposomes were first incubated with the his-tagged RGD peptide and then with both cell lines. Approximately 550 peptides were attached to each liposome. Liposomal uptake was assessed by examining the fluorescence in the cells after washing and lysis (to remove any effects of cargo self-quenching). As shown in Fig. 5b, a high liposome uptake was observed in the U87 cells incubated with the targeted Co-PoP liposomes, whereas negligible binding occurred with the MCF7 cells. As expected, without the RGD-targeting ligand no uptake occurred in either cell line. Inclusion of PEG-lipid in the liposome formulation resulted in liposomes that did not target to either cell line. It is probable that the presence of the PEG had the effect of obstructing the peptide, which is directly tethered to the bilayer surface. Binding was inhibited with the presence of excess free RGD peptide, which confirms the targeting specificity of the approach. Confocal microscopy substantiated these binding results (Fig. 5c). Although the FAM-labelled peptide was quenched by the PoP liposomes, sufficient signal remained to verify the binding of both the targeting peptide and the liposomal cargo. Both the cargo and the peptide were internalized and remained colocalized in the U87 cells. When the Co-PoP liposomes and targeting peptide were admixed immediately prior to incubation with the U87 cells, the targeting peptide itself bound to the U87 cells but did not have time to attach to the liposomes, which remained untargeted. The same result was observed for 2H-PoP

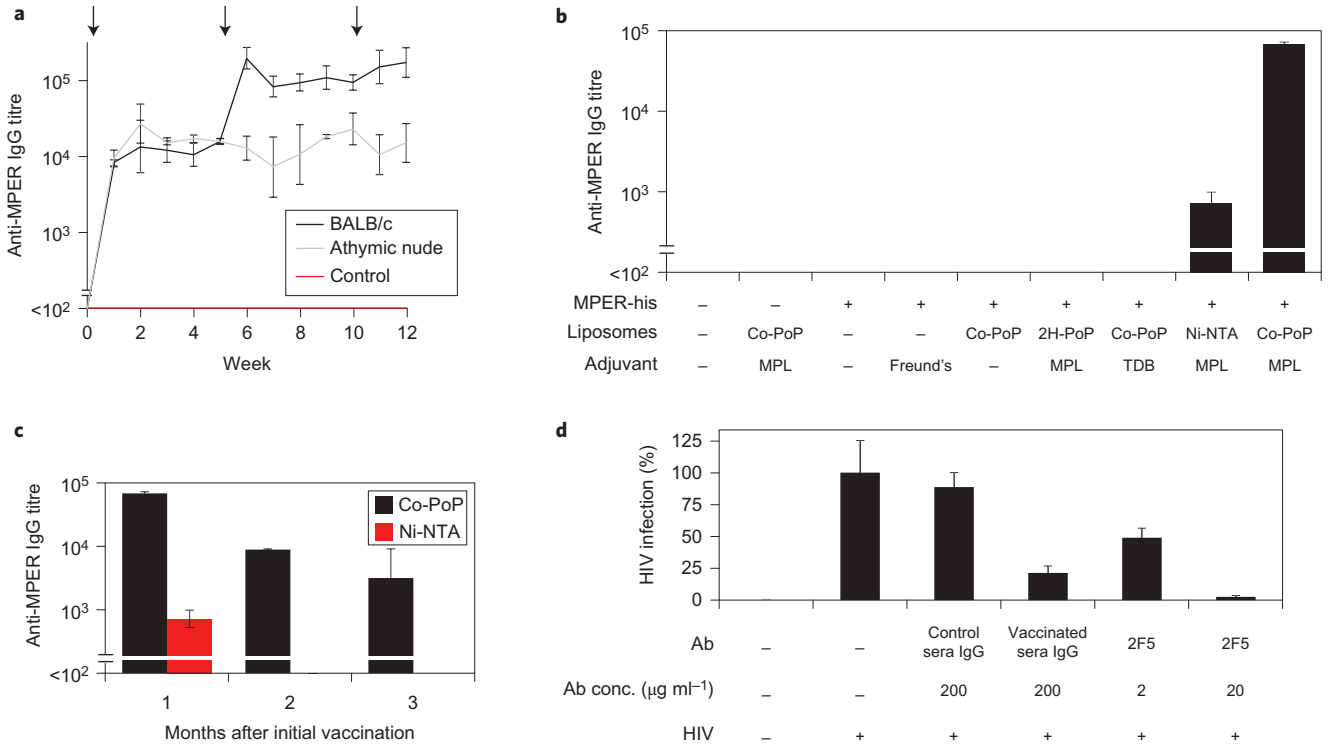

Figure 6 | HIV peptide vaccination using immunogenic Co-PoP liposomes. a, BALB/c or athymic nude mice were immunized with Co-PoP liposomes that contained 25 μg MPL and 25 μg his-tagged MPER peptide derived from the HIV gp41 envelope protein. The sera titres were assessed with ELISA using a biotinylated MPER peptide that lacked a his-tag and then probed with an anti-IgG secondary antibody. Arrows indicate the time of the vaccinations. Mean ± s.d. for $n = 4$ mice per group. **b**, Anti-MPER titre in BALB/c mice vaccinated as indicated. Mice were vaccinated on week 0 and week 2 and the serum was collected on week 4. Mean ± s.d. for $n = 4$ mice per group. **c**, Sustained anti-MPER titre in mice vaccinated with Co-PoP liposomes that contained MPL relative to Ni-NTA liposomes that contained MPL. Mean ± s.d. for $n = 4$ mice per group. **d**, Neutralization of HIV infection in TZM-bl cells in the presence of the indicated antibodies. After vaccination using Co-PoP, IgGs were purified from pooled mouse sera using Protein G. The broadly neutralizing antibody 2F5 was used as a control. Mean ± s.d. for $n = 3$.

liposomes, which did not bind the peptide. Peptide binding was maintained when the liposomes were formed with only 1 mol% Co-PoP (Supplementary Fig. 6a) and the selective binding to the U87 cells was maintained (Supplementary Fig. 6b). Cargo-loaded liposomes that incubated a his-tagged cyclic RGD (cRGD) moiety were injected intravenously into nude mice that bore U87 tumours. As shown in Fig. 5d, 45 minutes after the intravenous injection the targeted liposomes accumulated in tumours with a 2.5-fold avidity compared to that of the untargeted liposomes. These data show that Co-PoP liposomes can be loaded with cargo in the core of the liposome, be labelled with a his-tagged targeting peptide without inducing cargo leakage and be directed to molecular receptors expressed on cells that express specific surface proteins *in vitro* and *in vivo*.

Liposomes represent only a subset of all the types of nanomaterials used in biomedical applications[37]. Co-PoP was assessed as a generalized surface coating with a selective adhesion for his-tags. Gold nanoparticles were used as a model nanoparticle because these are used in numerous biological applications[38]. Using an established protocol to lipid-coat gold nanospheres[39], a citrate-stabilized 60 nm gold dispersion was used to hydrate a thin film of PoP lipid. On repeated centrifugation and resuspension, the citrate was displaced, which caused the nanospheres to aggregate (Supplementary Fig. 7a). However, in the presence of the PoP lipid, the nanospheres became coated and remained dispersible. The PoP-coated nanospheres had a slightly larger hydrodynamic size than the citrate-stabilized gold because of the bilayer coating on the gold (Supplementary Fig. 7b). The presence of the coating after his-tag binding did not influence the plasmonic peak of the gold at 540 nm, which demonstrates the mild nature of the ligand binding (Supplementary Fig. 7c). As shown in Supplementary Fig. 7d, only RGD-his Co-PoP-coated gold nanoparticles targeted U87 cells and free RGD inhibited the binding as determined by backscatter microscopy. Co-PoP gold alone and 2H-PoP-coated gold incubated with the RGD-his peptide were ineffective at targeting U87 cells.

Development of antigenic liposomes. Many of the monoclonal antibodies that broadly neutralize the human immunodeficiency virus (HIV) viral entry, such as 2F5, Z13 and 4E10, target a conserved linear epitope in the membrane proximal external region (MPER) of the gp41 envelope protein, which makes the MPER a prime target for HIV peptide vaccines[40,41]. However, it is exposed only during viral entry and attempts to use MPER peptides to generate neutralizing antibodies have faced challenges[42,43]. This has given rise to the paradigm that vaccination strategies should consider antibody interaction with the lipid bilayer in which the MPER is presented[44]. Recent efforts have made use of liposomes that contain the Toll-like receptor 4 (TLR-4) agonist monophosphoryl lipid A (MPL) combined with liposome-bound MPER peptide sequences[11,45,46]. However, the use of a simple anchoring technique based on the binding of MPER his-tagged polypeptides to Ni-NTA liposomes generated low antibody titres[47]. We set out to examine if the same approach could be enhanced with Co-PoP liposomes.

A liposomal-peptide vaccination system was used with the MPER-his sequence NEQELLELDKWASLWNGGKGG-HHHHHHH. The MPER-his peptide was bound to Co-PoP

liposomes that contained MPL. A single injection containing 25 μg MPER-his and 25 μg MPL was administered to BALB/c mice and to athymic nude mice. This elicited a titre on the order of 10^4 in both the BALB/c mice and the nude mice, which demonstrates a strong humoral immune response (Fig. 6a). This may be significant because HIV infects helper T cell populations, which makes responses mediated by B cells important. After a booster injection, the anti-MPER titre in athymic nude mice was unaffected, but in healthy mice there was a titre increase by an order of magnitude, which demonstrates a memory effect mediated by T cells. Thus, the vaccination protocol resulted in immunity mediated by both B cells and T cells. Interestingly, a recent vaccination study using MPL liposomes and a lipid-anchored Alzheimer's-related peptide demonstrated a response independent of T cells, without any boosting phenomenon[13]. That study used subcutaneous injections and lower MPL doses (12 versus 25 μg), which may account for the different immune responses.

Next, various liposome and adjuvant components were examined to better determine the specificity of the immune response (Fig. 6b). The MPER-his peptide did not elicit any antibodies when injected on its own, in Freund's complete adjuvant or along with 2H-PoP liposomes that contained MPL. When the peptide was administered with Co-PoP liposomes that lacked MPL, no antibodies were generated whatsoever. Another lipid adjuvant, trehalose dibehenate (TDB), also failed to elicit any antibody production. TDB does not act on TLR-4, which underlines the importance of MPL in the immune activation of the liposomal vaccine system. When MPER-his and Ni-NTA liposomes were used, a weak antibody titre of less than 10^3 was achieved, consistent with previous reports[47]. However, when Co-PoP liposomes were used, a titre two orders of magnitude greater was observed. Presumably, the stable binding of the peptide to the liposomes *in vivo* was directly responsible for this effect. The Co-PoP immunization strategy was effective, with antibody titres persisting for at least three months, whereas no antibodies were detected with Ni-NTA liposomes after one month (Fig. 6c).

Post-vaccination sera from mice were pooled and purified using Protein G agarose to yield purified immunoglobulin-G (IgG). This was then used to assess the inhibition of viral entry by HIV (Fig. 6d). When the purified IgG from vaccinated mice was used at a final concentration of 0.2 mg ml^{-1}, viral entry was inhibited by more than 75%. This efficacy of inhibition was greater than that of the broadly neutralizing monoclonal antibody 2F5 when incubated at a concentration of 2 μg ml^{-1}, but less than when incubated at 20 μg ml^{-1}. These data show the potential for a vaccination approach that makes use of Co-PoP liposomes with HIV-derived peptides to induce antibody generation that can prevent viral entry.

Conclusion

Co-PoP and structures formed thereof represent simple and versatile materials for binding his-tagged proteins and peptides. This coating can easily confer targeting or immunogenic properties to diverse materials, an approach that enables leverage of the his-tagged polypeptides produced through modern peptide synthesis and genetic engineering. These can be easily, reliably and stably inserted into Co-PoP liposomes and other bilayer-coated materials for applications in biological systems.

Materials

See the Supplementary Information for full details of the methods.

Polypeptides. Custom peptides were obtained from commercial sources (see Supplementary Table 1). The recombinant heptahistidine-tagged Cerulean–Venus fusion protein was produced as previously described[48].

PoP liposomes. 2H-PoP was synthesized as previously described[23]. The metallo-PoPs were generated by incubating excess metal acetates with PoP in methanol or tetrahydrofuran. Completion of the reaction was monitored by thin-layer chromatography. The solvent was then removed by rotary evaporation and PoP was extracted thrice with a chloroform:methanol:water mixture. The identity was confirmed by mass spectrometry. PoP liposomes were created using the thin-film method and extruded through 100 nm membranes using a handheld extruder. Stoichiometry approximations were based on the assumption that each ~100 nm liposome contained 80,000 lipids. For protein- and peptide-binding analyses, liposomes were formed with 10 mol% PoP along with 85 mol% DOPC (Avanti No. 850375P) and 5 mol% PEG-lipid (Avanti No. 880120P). Ni-NTA liposomes included 10 mol% Ni-NTA lipid dioleoylglycero-Ni-NTA (Avanti No. 790404P) as well as 10 mol% 2H-PoP. Sulforhodamine B (VWR No. 89139-502) liposomes contained 10 mol% PoP, 35 mol% cholesterol (Avanti No. 700000P), 55 mol% DOPC and PEG-lipid as indicated. For bilayer integrity, cell binding and *in vivo* studies, a 50 mM dye was used for lipid film hydration, whereas for microscopy studies a 10 mM dye was used. Free dye was removed by gel filtration.

Polypeptide binding. The fluorescent reporter protein (1 μg) was incubated with 20 μg liposomes in 200 μl PBS. Fluorescence in the FRET channel was measured and data were normalized to the FRET signal of the protein without the addition of liposomes. EMSA experiments were performed using 2.5 μg protein incubated with 50 μg liposomes. For imidazole displacement experiments, 1 μg reporter protein was bound to 20 μg liposomes. Imidazole was then titrated and the binding was assessed with fluorescence. For serum stability, 1 μg reporter protein was bound to 20 μg liposomes in 100 μl PBS and then an equal volume of FBS was added and the binding was monitored by fluorescence. Peptide binding was assessed with RGD-his FAM fluorophore quenching after incubation of 500 ng peptide with 20 μg liposomes.

Targeting experiments. U-87 cells (2×10^4) and MCF-7 cells (2×10^4) were seeded overnight in a 96-well plate. RGD-his peptide (500 ng) was bound with 20 μg liposomes loaded with sulforhodamine B, and then incubated with the cells for two hours. The media was removed, cells were washed and liposomal uptake was assessed by the fluorescence of sulforhodamine B after lysis with a 1% Triton X-100 solution. For confocal imaging, 10^4 cells were seeded overnight in a chamber slide and 20 μg liposomes were then added to the serum-containing media and incubated for two hours. The media was removed and the cells were washed prior to confocal microscopy. Animal procedures were conducted in accordance with the policies of the University at Buffalo Institutional Animal Care and Use Committee. Five-week-old female athymic nude mice that bore U87 flank tumours (~5 mm) were intravenously injected with 200 μl liposomes loaded with sulforhodamine B with or without cRGD-his. After 45 minutes, the mice were sacrificed and the organs were extracted, homogenized in a 0.2% Triton X-100 solution and the fluorescence assessed to determine the biodistribution.

Vaccinations. On days 0 and 14, eight-week-old female BALB/c mice (Harlan Laboratories) received hind ventral footpad injections that contained 25 μg MPER peptide in 50 μl sterile PBS. Where indicated, the injections also included 25 μg MPL incorporated into the liposomes (Avanti No. 699800P). The anti-MPER titre was assessed by enzyme-linked immunosorbent assay (ELISA) in 96-well streptavidin-coated plates (GBiosciences No. 130804). His-tag-free MPER biotin (1 μg) in 100 μl PBS that contained 0.1% Tween-20 (PBS-T) was incubated in the wells for two hours at 37 °C. Wells were washed and mouse sera were diluted in PBS that contained 0.1% casein and then incubated. Wells were then washed with PBS-T and goat anti-mouse IgG-HRP (GenScript No. A00160) was added. The wells were washed again with PBS-T before the addition of tetramethylbenzidine (Amresco No. J644). Titres were defined as the reciprocal serum dilution at which the absorbance at 450 nm exceeded the background by more than 0.05 absorbance units. Every sample was averaged from duplicate measurements.

Viral entry experiments. Viral entry experiments were carried out as previously described[49]. Sera from three mice immunized with MPER and Co-PoP liposomes were pooled and IgG was isolated using immobilized Protein G beads (VWR No. PI20398) according to manufacturer protocol. 2F5 was provided by the free NIH AIDS Reagent Program. Receptor cells (1×10^4 TZM-bl per well) were plated in a 96-well plate the day before infection. HIV (multiplicity of infection of 0.1) was incubated with antibodies for 30 minutes at 37 °C, added to the cells and spinoculated at 1,000*g* for one hour at 25 °C followed by a further incubation for two days at 37 °C. Cell viability and viral entry were assessed, respectively, using the CellTiter-Fluor (Promega) and One-Glo (Promega) assays according to manufacturer protocol.

Received 16 September 2014; accepted 16 March 2015; published online 20 April 2015

References

1. Brannon-Peppas, L. & Blanchette, J. O. Nanoparticle and targeted systems for cancer therapy. *Adv. Drug Deliv. Rev.* 206–212 (2012).
2. Purcell, A. W., McCluskey, J. & Rossjohn, J. More than one reason to rethink the use of peptides in vaccine design. *Nature Rev. Drug Discov.* **6,** 404–414 (2007).

3. Canalle, L. A., Löwik, D. W. P. M. & van Hest, J. C. M. Polypeptide-polymer bioconjugates. *Chem. Soc. Rev.* **39,** 329–353 (2010).
4. Nobs, L., Buchegger, F., Gurny, R. & Allémann, E. Current methods for attaching targeting ligands to liposomes and nanoparticles. *J. Pharm. Sci.* **93,** 1980–1992 (2004).
5. Algar, W. R. *et al.* The controlled display of biomolecules on nanoparticles: a challenge suited to bioorthogonal chemistry. *Bioconjug. Chem.* **22,** 825–858 (2011).
6. Sapra, P. & Allen, T. M. Ligand-targeted liposomal anticancer drugs. *Prog. Lipid Res.* **42,** 439–462 (2003).
7. Kirpotin, D. *et al.* Sterically stabilized anti-HER2 immunoliposomes: design and targeting to human breast cancer cells *in vitro*. *Biochemistry* **36,** 66–75 (1997).
8. Yang, T. *et al.* Preparation and evaluation of paclitaxel-loaded PEGylated immunoliposome. *J. Control. Release* **120,** 169–177 (2007).
9. Mastrobattista, E., Koning, G. A. & Storm, G. Immunoliposomes for the targeted delivery of antitumor drugs. *Adv. Drug Deliv. Rev.* **40,** 103–127 (1999).
10. Said Hassane, F., Frisch, B. & Schuber, F. Targeted liposomes: convenient coupling of ligands to preformed vesicles using 'click chemistry'. *Bioconjug. Chem.* **17,** 849–854 (2006).
11. Watson, D. S. & Szoka, F. C. Jr. Role of lipid structure in the humoral immune response in mice to covalent lipid–peptides from the membrane proximal region of HIV-1 gp41. *Vaccine* **27,** 4672–4683 (2009).
12. Liang, M. T., Davies, N. M. & Toth, I. Encapsulation of lipopeptides within liposomes: effect of number of lipid chains, chain length and method of liposome preparation. *Int. J. Pharm.* **301,** 247–254 (2005).
13. Pihlgren, M. *et al.* TLR4- and TRIF-dependent stimulation of B lymphocytes by peptide liposomes enables T cell-independent isotype switch in mice. *Blood* **121,** 85–94 (2013).
14. Blanco-Canosa, J. B. *et al.* Recent progress in the bioconjugation of quantum dots. *Coord. Chem. Rev.* **263–264,** 101–137 (2014).
15. Terpe, K. Overview of tag protein fusions: from molecular and biochemical fundamentals to commercial systems. *Appl. Microbiol. Biotechnol.* **60,** 523–533 (2003).
16. Arnau, J., Lauritzen, C., Petersen, G. E. & Pedersen, J. Current strategies for the use of affinity tags and tag removal for the purification of recombinant proteins. *Protein Expres. Purif.* **48,** 1–13 (2006).
17. Kubalek, E. W., Le Grice, S. F. J. & Brown, P. O. Two-dimensional crystallization of histidine-tagged, HIV-1 reverse transcriptase promoted by a novel nickel-chelating lipid. *J. Struct. Biol.* **113,** 117–123 (1994).
18. Dorn, I. T., Neumaier, K. R. & Tampé, R. Molecular recognition of histidine-tagged molecules by metal-chelating lipids monitored by fluorescence energy transfer and correlation spectroscopy. *J. Am. Chem. Soc.* **120,** 2753–2763 (1998).
19. Hussein, W. M., Ross, B. P., Landsberg, M. J., Hankamer, B. & McGeary, R. P. Synthetic approaches to functionalized lipids for protein monolayer crystallizations. *Curr. Org. Chem.* **13,** 1378–1405 (2009).
20. Platt, V. *et al.* Influence of multivalent nitrilotriacetic acid lipid–ligand affinity on the circulation half-life in mice of a liposome-attached his_6-protein. *Bioconjug. Chem.* **21,** 892–902 (2010).
21. Rüger, R., Müller, D., Fahr, A. & Kontermann, R. E. *In vitro* characterization of binding and stability of single-chain Fv Ni-NTA-liposomes. *J. Drug Target.* **14,** 576–582 (2006).
22. Xie, J., Lee, S. & Chen, X. Nanoparticle-based theranostic agents. *Adv. Drug Deliv. Rev.* **62,** 1064–1079 (2010).
23. Lovell, J. F. *et al.* Porphysome nanovesicles generated by porphyrin bilayers for use as multimodal biophotonic contrast agents. *Nature Mater.* **10,** 324–332 (2011).
24. Lovell, J. F. *et al.* Enzymatic regioselection for the synthesis and biodegradation of porphysome nanovesicles. *Angew. Chem. Int. Ed.* **51,** 2429–2433 (2012).
25. Carter, K. A. *et al.* Porphyrin–phospholipid liposomes permeabilized by near-infrared light. *Nature Commun.* **5,** 3546 (2014).
26. Rieffel, J. *et al.* Hexamodal imaging with porphyrin–phospholipid-coated upconversion nanoparticles. *Adv. Mater.* **27,** 1785–1790 (2015).
27. Pasternack, R. F., Francesconi, L., Raff, D. & Spiro, E. Aggregation of nickel(II), copper(II), and zinc(II) derivatives of water-soluble porphyrins. *Inorg. Chem.* **12,** 2606–2611 (1973).
28. Constable, E. C. & Housecroft, C. E. Coordination chemistry: the scientific legacy of Alfred Werner. *Chem. Soc. Rev.* **42,** 1429–1439 (2013).
29. Wegner, S. V. & Spatz, J. P. Cobalt(III) as a stable and inert mediator ion between NTA and his_6-tagged proteins. *Angew. Chem. Int. Ed.* **52,** 7593–7596 (2013).
30. Terekhov, S. N., Galievsky, V. A., Chirvony, V. S. & Turpin, P-Y. Resonance Raman and absorption characterization of cationic Co(II)-porphyrin in its complexes with nucleic acids: binding modes, nucleic base specificity and role of water in Co(II) oxidation processes. *J. Raman Spectrosc.* **36,** 962–973 (2005).
31. Ruoslahti, E. Peptides as targeting elements and tissue penetration devices for nanoparticles. *Adv. Mater.* **24,** 3747–3756 (2012).
32. Pasqualini, R., Koivunen, E. & Ruoslahti, E. Alpha v integrins as receptors for tumor targeting by circulating ligands. *Nature Biotechnol.* **15,** 542–546 (1997).
33. Danhier, F., Breton, A. L. & Préat, V. RGD-based strategies to target alpha (v) beta(3) integrin in cancer therapy and diagnosis. *Mol. Pharm.* **9,** 2961–2973 (2012).
34. Bloch, S. *et al.* Targeting beta-3 integrin using a linear hexapeptide labeled with a near-infrared fluorescent molecular probe. *Mol. Pharm.* **3,** 539–549 (2006).
35. Cai, W. *et al.* Peptide-labeled near-infrared quantum dots for imaging tumor vasculature in living subjects. *Nano Lett.* **6,** 669–676 (2006).
36. Hong, G. *et al.* Near-infrared-fluorescence-enhanced molecular imaging of live cells on gold substrates. *Angew. Chem. Int. Ed.* **50,** 4644–4648 (2011).
37. Janib, S. M., Moses, A. S. & MacKay, J. A. Imaging and drug delivery using theranostic nanoparticles. *Adv. Drug Deliv. Rev.* **62,** 1052–1063 (2010).
38. Sperling, R. A., Gil, P. R., Zhang, F., Zanella, M. & Parak, W. J. Biological applications of gold nanoparticles. *Chem. Soc. Rev.* **37,** 1896–1908 (2008).
39. Tam, N. C. M., Scott, B. M. T., Voicu, D., Wilson, B. C. & Zheng, G. Facile synthesis of Raman active phospholipid gold nanoparticles. *Bioconjug. Chem.* **21,** 2178–2182 (2010).
40. Zwick, M. B. *et al.* Broadly neutralizing antibodies targeted to the membrane-proximal external region of human immunodeficiency virus Type 1 glycoprotein gp41. *J. Virol.* **75,** 10892–10905 (2001).
41. Zwick, M. B. The membrane-proximal external region of HIV-1 gp41: a vaccine target worth exploring. *AIDS* **19,** 1725–1737 (2005).
42. Montero, M., van Houten, N. E., Wang, X. & Scott, J. K. The membrane-proximal external region of the human immunodeficiency virus Type 1 envelope: dominant site of antibody neutralization and target for vaccine design. *Microbiol. Mol. Biol. Rev.* **72,** 54–84 (2008).
43. Burton, D. R. *et al.* HIV vaccine design and the neutralizing antibody problem. *Nature Immunol.* **5,** 233–236 (2004).
44. Alam, S. M. *et al.* Role of HIV membrane in neutralization by two broadly neutralizing antibodies. *Proc. Natl Acad. Sci.* **106,** 20234–20239 (2009).
45. Matyas, G. R. *et al.* Neutralizing antibodies induced by liposomal HIV-1 glycoprotein 41 peptide simultaneously bind to both the 2F5 or 4E10 epitope and lipid epitopes. *AIDS* **23,** 2069–2077 (2009).
46. Verkoczy, L. *et al.* Induction of HIV-1 broad neutralizing antibodies in 2f5 knock-in mice: selection against membrane proximal external region–associated autoreactivity limits T-dependent responses. *J. Immunol.* **191,** 2538–2550 (2013).
47. Watson, D. S., Platt, V. M., Cao, L., Venditto, V. J. & Szoka, F. C. Antibody response to polyhistidine-tagged peptide and protein antigens attached to liposomes via lipid-linked nitrilotriacetice acid in mice. *Clin. Vaccine Immunol.* **18,** 289–297 (2011).
48. Dayananda, K. M., Gogia, S. & Neelamegham, S. *Escherichia coli*-derived von Willebrand factor-A2 domain fluorescence/Förster resonance energy transfer proteins that quantify ADAMTS13 activity. *Anal. Biochem.* **410,** 206–213 (2011).
49. Yi, H. A., Diaz-Aguilar, B., Bridon, D., Quraishi, O. & Jacobs, A. Permanent inhibition of viral entry by covalent entrapment of HIV gp41 on the virus surface. *Biochemistry* **50,** 6966–6972 (2011).

Acknowledgements

The authors thank J. R. Morrow and R. B. Bankert for valuable discussions, A. Siegel for assistance with confocal microscopy and the NIH AIDS Reagent Program. This work was supported by grants from the National Institutes of Health (R01EB017270, DP5OD017898 and HL77258).

Author contributions

S.G. and S.N. designed and produced the his-tagged fluorescence protein reporter. S.S. performed the synthesis, chemical characterization, binding, targeting and immunization experiments. J.G. led the animal experiments. A.J. and H.A.Y. carried out the HIV entry inhibition experiments. S.S. and J.F.L. conceived the project, interpreted the data and wrote the manuscript.

Additional information

Supplementary information is available in the online version of the paper. Reprints and permissions information is available online at www.nature.com/reprints. Correspondence and requests for materials should be addressed to J.F.L.

Competing financial interests

The authors declare no competing financial interests.